FULL PAPER

Dalton
www.rsc.org/dalton

Phosphorus carbides: theory and experiment † ‡

F. Claeyssens, G. M. Fuge, N. L. Allan, P. W. May and M. N. R. Ashfold
School of Chemistry, University of Bristol, Bristol, UK BS8 1TS

Received 23rd February 2004, Accepted 6th April 2004
First published as an Advance Article on the web 26th July 2004

The recent finding that radio frequency plasma activation of CH_4/PH_3 gas mixtures can yield films with P : C ratios ≤ 3 has served to trigger further research into new 'phosphorus carbide' materials. Theoretical and experimental results relating to periodic and amorphous materials, respectively, are presented here: (i) The electronic structure and stability of different crystalline phosphorus carbide P_xC_y phases have been studied using first-principles density-functional theory. Calculations have been carried out for P_4C_{3+8n} (n = 0–4), PC, and PC_3 and the most likely periodic structures examined in detail. Particular attention is paid to the composition PC_3, for which there are several possibilities of similar energy. (ii) Recent experimental efforts have involved use of pulsed laser ablation methods to produce hydrogen-free phosphorus carbide thin films. Mechanically hard, electrically conducting diamond like carbon films containing 0–~26 at.% P have been deposited on both Si and quartz substrates by 193 nm PLA of graphite/phosphorus targets (containing varying percentages of phosphorus), at a range of substrate temperatures (T_{sub} = 298–700 K), in vacuum, and analysed *via* laser Raman and X-ray photoelectron spectroscopy.

Introduction

Binary nitrides have been the subject of major research efforts in recent years. Carbon nitride (C_3N_4), in particular, has attracted much attention, as a result of theoretical predictions [1] that it should possess a hardness comparable to diamond, combined with high toughness, and excellent tribological, chemical and electrical properties. Disappointingly, synthesis of crystalline carbon nitride has proved to be far from straightforward and so far only small amounts of crystalline material have been prepared.[2] The products of most physical processes used for carbon nitride deposition, such as pulsed laser ablation (PLA),[3] cathodic arc deposition [4] and chemical vapour deposition (CVD),[5] have been amorphous films containing low (1–10%) percentages of nitrogen. Thus nitrogen incorporation into the carbon lattice appears to be very difficult, although exciting synthetic routes towards graphite-like C_3N_4 materials have been recently developed.[6,7]

Given the current experimental impasse in the production of either crystalline or amorphous carbon nitride with high nitrogen content, it is of interest to turn to possible phosphorus analogues. In contrast to the nitrogen case, amorphous thin films with a wide range of P : C compositions up to a molar ratio of 3 : 1 have been produced *via* capacitively-coupled radio frequency (RF) plasma deposition from PH_3/CH_4 gas mixtures.[8] These films also contain an amount of hydrogen (~10%), from the gas mixture, and are readily oxidised, as revealed by secondary ions mass spectrometry (SIMS) and X-ray photoelectron spectroscopy (XPS). UV-VIS spectroscopy reveals an absorption threshold at ~2.7 eV for films with small P : C ratios, which shifts progressively to ~2 eV as the phosphorus content increases to a P : C ratio of ~3 : 1.

These developments have prompted a number of experimental and theoretical studies of phosphorus carbide thin films. In this paper we discuss *ab initio* studies of some crystalline phosphorus carbides [9,10] including P_4C_{3+8n} (n = 0–4), PC and PC_3, with emphasis on the last of these stoichiometries, and compare the predicted structures for each compound. We also report recent experimental studies that focus on production of hydrogen-free phosphorus carbide films *via* PLA methods, and the subsequent characterisation of these films.[11]

Theoretical

Computational details

Most calculations were carried out using periodic density-functional theory (DFT) and plane waves in the generalized gradient approximation (GGA) with the Perdew–Wang exchange correlation functional,[12] as implemented in the CASTEP code.[13] The ultra-soft Vanderbilt pseudo-potentials [14] were used together with an energy cut-off for the plane waves of 310 eV. Checks were carried out to ensure that all results were well converged with respect to the real space grid, Brillouin zone sampling and basis set size. In the final stages of the optimisation all symmetry constraints were removed. In our previous work [9,10] on P_4C_3 and P_4C_{3+8n} all calculations were also repeated using periodic numerical atomic orbitals DFT as implemented in the SIESTA code [15] and using the exchange–correlation functional of Perdew, Burke and Ernzerhof.[16] We noted no substantial differences between the results of the two methods and so here we concentrate on plane-wave calculations.

Results

Using periodic density functional theory, we have previously examined possible crystalline structures with stoichiometries P_4C_3,[9] P_4C_{11}, P_4C_{19}, P_4C_{27} and P_4C_{35} [10] and have presented [17,18] preliminary results for PC. Throughout we have been guided in our choices both of composition and of initial choice of structures by those proposed for the corresponding nitrogen analogues.[1,19,20] In this section we extend these studies and, in particular, examine composition PC_3 in detail, comparing calculated periodic structures with that suggested [21] for C_3N.

The lowest energy structure for P_4C_3 is the diamond-like 'pseudo-cubic' defect zinc blende, as shown in Fig. 1. Every P atom is bonded to three C atoms and every carbon to four P atoms. In general, structures low in energy for C_3N_4 are high in energy for P_4C_3, consistent with the molecular chemistries of N and P where it is well established [22] that phosphorus exhibits a much more marked preference than nitrogen for pyramidal coordination and thus for single rather than multiple bond formation. For C_3N_4, the cubic, α- and β-C_3N_4 structures

† Based on the presentation given at Dalton Discussion No. 7, 5–7th July 2004, University of St Andrews, UK.
‡ Electronic supplementary information (ESI) available: Space group information and optimised basis atom positions for hypothetical structures (A)–(H) for PC_3. See http://www.rsc.org/suppdata/dt/b4/b402740j/

DOI: 10.1039/b402740j

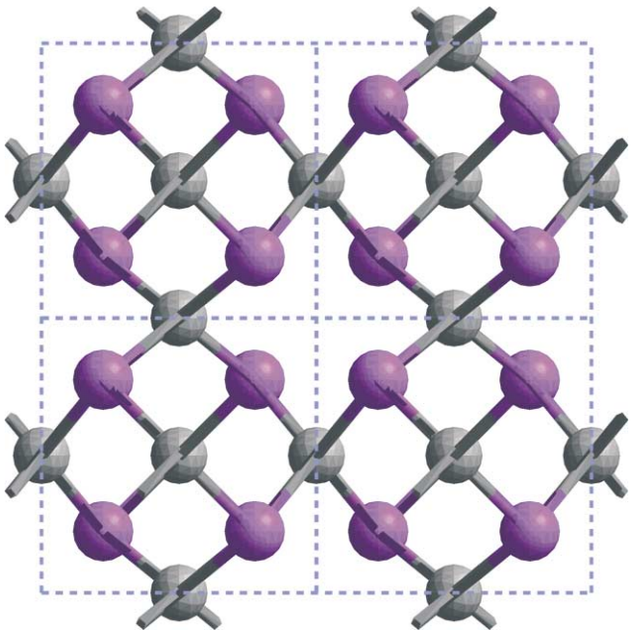

Fig. 1 Crystal structure of the pseudo-cubic phase of P_4C_3. Grey and purple spheres denote C and P atoms, respectively. The dashed blue line indicates the unit cell.

are each more stable than the pseudo-cubic. This reversal of stability is linked to differences in the CPC (CNC) bond angles between the different structures. These angles are all considerably larger (typically between 110 and 115°) in the α-, β-, and cubic phases than those in the pseudo-cubic, all of which are ≈104° and so closer to the CPC bond angle of 99° adopted in, for example, $P(CH_3)_3$.

For compositions P_4C_{3+8n} ($n > 0$) defect graphitic phases are lowest in energy.[10] An example is shown for P_4C_{11} in Fig. 2. It is tempting to link the enhanced stability of these graphitic structures (relative to P_4C_3) directly to the larger carbon content. P–C bonds are significantly weaker than C–C bonds and the graphitic forms of P_4C_{11} have an appreciably higher ratio of C–C : P–C bonds than does the pseudo-cubic. In addition there is also an appreciable mismatch between the lattice parameters of diamond and that of pseudo-cubic P_4C_3, suggesting a mismatch-induced stress in diamond-like P_4C_{11}. This mismatch is less important for the lower-dimensional graphitic structures. The lowest energy graphitic structure illustrated in Fig. 2 retains a chain of C_6 rings; in contrast to other possible structures,[10] some carbons are bonded to three phosphorus atoms. It is also worth noting that the layers in these structures show considerable distortion from 'ideal', planar graphitic structures and there are some short interlayer P–P interactions (≈2.4 Å).

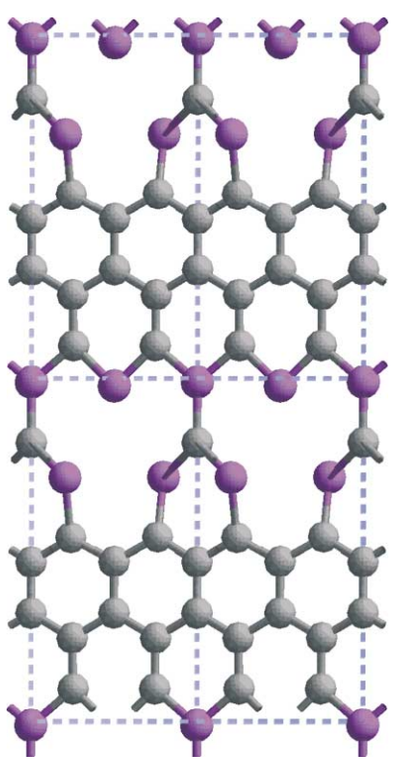

Fig. 2 Crystal structure of the lowest energy phase of P_4C_{11}. Atoms and unit cell indicated as in Fig. 1.

For PC one of the most stable crystalline structure contains layers with the bonding motif shown in Fig. 3; individual layers are linked to form bilayers by C–C bonds. The optimised structure (Fig. 4) is that adopted by GaSe,[17] as found also by Zheng *et al.*[23] Table 1 lists calculated properties of the lowest energy structures for P_4C_3 and PC. In both, carbon and phosphorus atoms are four- and three-fold coordinate, respectively. Also present in both is an sp^3-bonded network, three-dimensional for P_4C_3, but two-dimensional for PC. The CPC angle in the GaSe structure adopted by PC is ≈101°, which is close to the bond angle for tetrahedral coordination preferred by phosphorus.

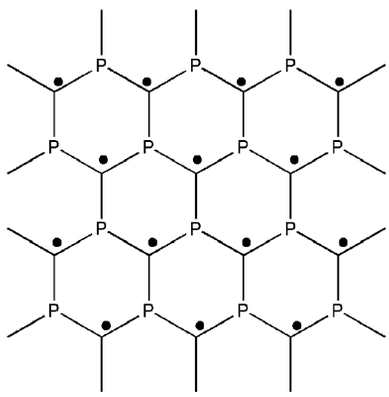

Fig. 3 Structural motif present in each layer in the lowest energy (GaSe) structure of PC. Each carbon atom forms an additional bond with a carbon in the second layer present in the bilayer.

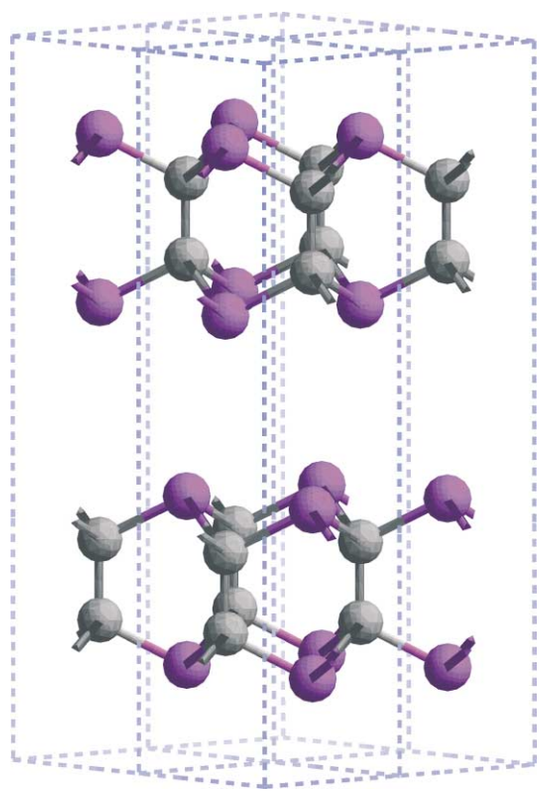

Fig. 4 Crystal structure of the GaSe phase of PC. Atoms and unit cell indicated as in Fig. 1.

Table 1 Calculated properties of the calculated minimum energy crystalline structures for P_4C_3 and PC

Structure	P_4C_3	PC
Space group	$P\bar{4}3/m$ (no. 215)	$P63/mmc$ (no. 194)
Volume per formula unit/Å^3	70.45	23.63
a/Å	4.130	2.847
b/Å	4.130	2.847
c/Å	4.130	13.465
α/°	90.0	90.0
β/°	90.0	90.0
γ/°	90.0	120.0
Band gap/eV	0.00	1.41
Bulk modulus/GPa	156	64

While there are C–C bonds in the GaSe PC structure, there are none in pseudo-cubic P_4C_3. Whereas the predicted lowest energy structure for P_4C_3 is quite different from that for C_3N_4, those for CN [20] and PC are the same. Calculated bulk moduli of the P_4C_3 and PC structures are 156 and 64 GPa, respectively, indicating, not unexpectedly, that the layered, graphitic-like PC structure is less hard than the 3-D pseudo-cubic P_4C_3 structure.

We start our hunt for possible PC_3 structures keeping in mind that PC_3 units can be formed from P_2C_2 (PC × 2) by replacing one phosphorus with a carbon atom. The lowest energy structure we have found is based on the motif (I) shown in Fig. 5, and so is very different from that predicted for PC. It is graphitic-like with an orthorhombic unit cell (space group $Pmm2_1$) and retains the C_6 ring also present in the lowest energy form of P_4C_{11}. In contrast to all the structures examined so far, the phosphorus atoms in (I) are formally hypervalent; the P atoms are four-coordinate to three carbons and one phosphorus atom, and there are P–P bonds between the layers. A 3D-network is formed with P–P bonds (2.28 Å) between all layers, as is clear from Fig. 6(A). This structure is quite different from the flat N-substituted graphite structure predicted for C_3N by Sandré *et al.*[21] The hypervalent P atoms adopt an approximately tetrahedral geometry and so the individual planes deviate substantially from planarity, as is also evident in Fig. 6(A). Table 2 collects together the optimised lattice parameters and

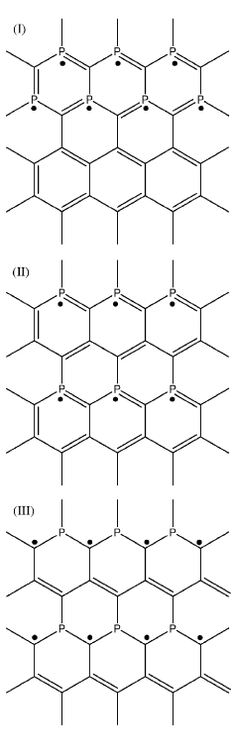

Fig. 5 Structural motifs (I)–(III) present in the set of possible structures considered for PC_3. Filled circles denote atoms which bond to atoms in an adjacent layer. Motifs (I) and (II) contain formally hypervalent phosphorus.

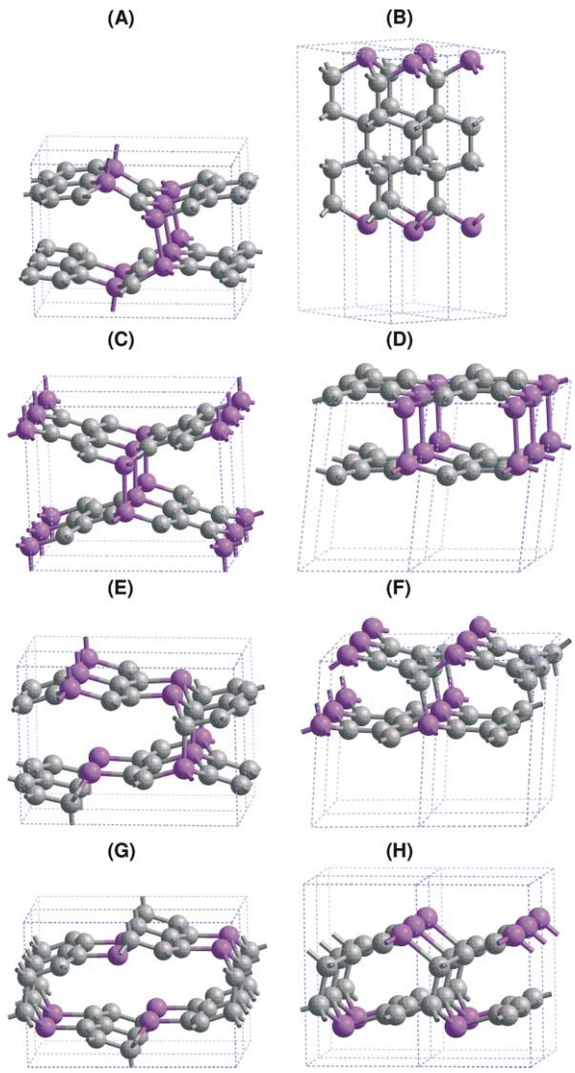

Fig. 6 Crystal structures of possible phases of PC_3. Labels (A)–(H) are the same as in Table 2. Atoms and unit cells indicated as in Fig. 1.

corresponding energies for this and all the other structures we have considered for PC_3. The supplementary information ‡ lists the space groups and the corresponding positions of the atoms in the asymmetric unit.

The lowest energy PC_3 structure is thus substantially different from that for the GaSe structure predicted for PC. A possible structure for PC_3, which, unlike (A), is related to GaSe, comprises layers of stoichiometry PC with the bonding motif shown in Fig. 3 as well as layers comprised only of sp^3-bonded carbon in chair conformations. The unit cell contains four layers (PC, C, C, PC), with the pure carbon layers adjacent to each other. Carbon and phosphorus atoms are four- and three-fold coordinate, respectively. The optimised structure (B) is the third lowest in energy of those we have examined and is shown in Fig. 6(B). This is also the most dense of all the structures we have examined and, unlike the GaSe structure itself, contains a three-dimensional sp^3-bonded network.

The second-lowest structure, close in energy to (A), is one member of a further subset of graphitic structures, similar to (A) but with different arrangements of the C and P atoms within each layer and without the C_6 rings that are present in (A). In all members of this subset there is intra- as well as interlayer bonding. There are two possibilities for an individual layer. In the first motif, which we refer to as 'pattern II' (Fig. 5), each carbon is three-coordinate to P (all in the layer) while the P is again hypervalent, being four coordinate with three intra-layer bonds to C and one interlayer bond (as in (A)). In the second, the phosphorus is three-coordinate to C (all within the

Table 2 Calculated volumes, energies and lattice parameters for the possible structures for PC_3 considered in this paper. Structure labels are as in Fig. 6. Space group information and optimised basis atom positions are in the ESI ‡

Structure	(A)	(B)	(C)	(D)
Energy per formula unit/eV	−647.99	−647.73	−647.83	−647.72
Volume per formula unit/Å^3	42.77	35.84	46.52	42.68
a/Å	2.636	2.658	2.638	4.646
b/Å	9.138	2.658	9.034	2.639
c/Å	7.103	11.715	7.809	7.045
α/°	90.0	89.9	90.0	90.0
β/°	90.0	90.0	90.0	99.0
γ/°	90.0	120.0	90.0	90.0

Structure	(E)	(F)	(G)	(H)
Energy per formula unit/eV	−647.59	−647.57	−647.15	−647.32
Volume per formula unit/Å^3	40.21	43.19	38.28	42.74
a/Å	2.615	2.653	9.135	4.507
b/Å	9.090	7.138	6.466	2.621
c/Å	6.776	4.584	2.593	7.236
α/°	90.0	84.3	90.0	90.0
β/°	90.0	90.0	90.0	90.5
γ/°	90.0	90.0	90.0	89.9

layer) while carbon is four-coordinate with three intra-layer bonds to P and one interlayer bond. We refer to this bonding motif, also shown in Fig. 5, as 'pattern III'. There is a lone pair of electrons on the P atom.

Bilayers can be constructed from two 'pattern II' layers (which we denote 'bilayer 1' and which contain interlayer P–P bonds) or from two 'pattern III' layers ('bilayer 2', containing interlayer C–C bonds), or by combining a 'pattern II' layer with a 'pattern III' ('bilayer 3', containing interlayer P–C bonds). We have considered three possibilities involving AA stacking of bilayers, with interlayer P–P, P–C and C–C bonds, respectively. The resulting optimised periodic structures are shown in Fig. 6 (structures (D), (F) and (H)).

Further structures in this subset are based on the same bonding motifs, pattern II and pattern III (Fig. 5) but, in contrast to the bilayer structures, contain three-dimensional networks, in which each layer forms interlayer bonds to *both* its neighbours. Again three modifications have been investigated. In the first, all individual layers are 'pattern II' and there are P–P bonds between all layers (structure (C)). Secondly, all individual layers can be 'pattern III' with C–C bonds between all layers (structure (G)). In the third modification (structure (E)), every 'pattern II' layer has layers of type 'pattern III' above and below, and all interlayer bonds are P–C. Optimised structures are again shown in Fig. 6. The calculated energies of all of these structures are close in energy to those of the corresponding bilayer structures. Structures with the same interlayer connectivity (*i.e.*, pairs (C) and (D), (E) and (F), and (G) and (H)) are closest in energy, with the (C) and (D) pair – involving hypervalent P atoms and interlayer P–P bonds – lying at lowest energy. The driving force for this difference in energy ordering appears to be the strain induced by the combination of relatively long P–C and relatively short C=C bonds within the layers based on 'pattern II'. In summary, there are several possible structures for PC_3 close in energy, and some are sufficiently close structurally to suggest facile transformation pathways between them.

The lowest energy structure (A) for PC_3 thus provides some striking contrasts with those predicted for other stoichiometries.[9,10,17] Like P_4C_{11}, the nearest in composition that we have studied previously,[10] the lowest energy structure is graphitic. Indeed, all compositions richer in carbon than P_4C_{11} investigated thus far are found to have graphitic forms lowest in energy, while those with C : P ratios < 2.75 exhibit sp^3-network structures. Unlike P_4C_{11}, PC_3 is predicted to be a three-dimensional, relatively low-density structure with hypervalent P, sp^2-hybridised C atoms, and direct interlayer P–P bonds. For P_4C_3, the lowest energy predicted structure is also three-dimensional but is diamond-like, of relatively high density, and does not contain P–P bonds. The lowest energy structure for PC is also of relatively low density, but is structurally distinct with C–C bonds between the individual layers of sp^3-bonded bilayers. Overall, a rich range of structures and phosphorus environments is clearly available for P_yC_x depending on (local) composition.

There are essentially three types of local phosphorus environment in all of the different structures identified that involve P atoms which are more than two-coordinate. These are shown schematically in Fig. 7. In the first, phosphorus is three-fold coordinate and a pyramidal geometry is adopted. The CPC bond angle is typically ≈97°. Typical P–C bond lengths are ≈1.77 Å. These values reflect the stress-induced mismatch in PC_3, since the corresponding values in 'diamond-like' pseudo-cubic P_4C_3 are 104° and 1.86 Å, respectively; there is a considerable compression of the P–C bond. P–C bond lengths where the P is two-coordinate (in, for example, the low energy graphitic form of P_4C_{11}) are ≈1.76 Å. The other two local environments (also shown in Fig. 7) both involve hypervalent phosphorus. The P atoms are four-fold coordinate in an approximately tetrahedral arrangement either to three C atoms and one P, or to four carbons. This is similar to that adopted in several P-containing organic molecules such as $PhP(PMe_2{=}C(SiMe_3)_2)_2]$,[24] CPC angles in all cases are in the range 109–116°, and P–C bond lengths can be significantly shorter (~1.67 Å) if, by so doing, they reduce the mismatch with the C–C bonds.

In the lowest energy P_3C structure (A), P–C bond lengths are 1.67–1.77 Å, with the 1.77 Å bonds those that connect P_3C_3 rings with C_6 rings. The P–P interlayer bond distance is 2.28 Å. The P–C bond lengths in layers based on 'pattern I' are similar, since both (A) and this pattern contain hypervalent

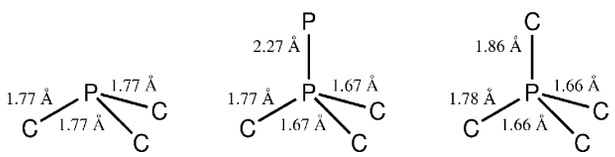

Fig. 7 The three local phosphorus environments found in the optimised structures for PC_3, associated with three-coordinate (pyramidal) (structure (B)), and hypervalent phosphorus atoms (P_2C_3 tetrahedral unit from structure (A), PC_4 unit from structure (E)). CPC angles associated with the three-coordinate phosphorus are ≈97°. CPC and CPP angles associated with the hypervalent P atoms lie in the ranges 109–116 and 106–112°, respectively.

phosphorus. In layers based on 'pattern II', however, the P–C bonds associated with the pyramidal P atoms are longer and the size mismatch with the C–C bonds is greater, suggesting greater strain in structures based on this motif.

One distinguishing feature between the carbon nitrides and the phosphorus carbides is the polarity of the bonds. Whereas C–N bonds are polarised $C^{\delta+}$–$N^{\delta-}$, the direction of polarisation is reversed in the P analogues ($P^{\delta+}$–$C^{\delta-}$), as is clear from the calculated Mulliken populations. The charge polarisation is a function of environment. For example, the Mulliken charge on hypervalent P is more positive than for three-coordinate phosphorus. In structure (E), where every bilayer is constructed from one layer of type 'pattern II' and a second 'pattern III' layer, there is a charge transfer to the 'pattern III' layer from the 'pattern II' layer indicating that the layer with hypervalent P carries a net positive charge. Thus there is a dipole perpendicular to the layers along the *c*-axis.

We have calculated the band structure for the lowest energy structures for P_4C_3, PC and PC_3. Using GGA, P_4C_3 is calculated to be metallic, while PC and PC_3 are insulators with direct band gaps of 1.41 and 1.51 eV, respectively. DFT calculations are notorious for underestimating the band gap, so the reported values should be considered as lower limits for the respective band gaps.[25]

The cohesive energies follow the expected trend: $P_4C_3 < PC < PC_3$. The energy of formation of these three structures has also been estimated, using in addition the calculated energies of elemental carbon (diamond structure) and phosphorus (black phosphorus). The heat of formation of PC_3 is positive (≈2 eV per formula unit) but this should not preclude formation of the proposed structures *via* a kinetically controlled pathway.

Experimental

Two experimental routes to forming carbon/phosphorus containing thin films have been investigated in Bristol. One has employed capacitively-coupled radio-frequency (RF) plasma deposition from PH_3/CH_4 gas mixtures.[8,26,27] Amorphous films with a wide spread of P : C ratios – ranging from 0 to ~3 – were obtained by appropriate choice of feedstock gas mixing ratio, deposition conditions, *etc.* Microcombustion analysis confirmed the expected presence of some (~10%) hydrogen in the deposited material.

Pulsed laser ablation (PLA) provides an attractive alternative route to depositing H-free phosphorus containing diamond-like-carbon (P-DLC) films.[11,17] 52 mm-diameter disk targets were prepared from intimately mixed finely powdered samples of graphite and red phosphorus powder using a hydraulic press, and subsequently polished to obtain a smooth, flat surface. Four targets were prepared, containing, respectively, 10, 20, 30 and 50% P by weight (or 4.1, 8.8, 14.2 and 27.9% P in terms of total atom number density). The selected target was mounted on a rotation stage within a stainless steel chamber evacuated to ~10^{-6} Torr. The output of an ArF (193 nm) excimer laser (Lambda-Physik, Compex 201, 10 Hz repetition rate) was focussed (450 mm f.l. fused silica lens) onto the target; the focal spot size on the target was ~1 mm^2, thus yielding incident fluences, *F*, in the range 4–12 J cm^{-2}. The substrate of choice (n-type single crystal (100) Si, or quartz (each ~1 cm^2 in area)) was mounted so that its front face was perpendicular to the target surface normal and 80 mm from the focal spot, on a purpose-designed holder that was itself positioned immediately in front of a 15 W projector light-bulb heater that enabled deposition at any user-selected substrate temperature $T_{sub} \leq 700$ K.

The resulting P-DLC films were analysed by laser Raman spectroscopy (LRS) employing a Renishaw 2000 system and an excitation wavelength of 514.5 nm, XPS (Fisons Instruments VG Escascope, Mg-Kα (1253.6 eV) source, analyser energy resolution of ~0.9 eV), and scanning electron microscopy (JEOL JSM 5600 LV scanning electron microscope). Spectroscopic ellipsometry was performed on films deposited on Si (J.A. Woollam VASE ellipsometer), at five incident angles between 55 and 75°, yielding values for Δ and Ψ over the spectral range of 200–1000 nm. Film optical constants (*n*, *k*) and the thickness were derived using a model of amorphous semiconductor on 0.5 mm thick crystalline Si, with the semiconductor layer described using the Tauc–Lorentz model.[28] All P-DLC films grown in this work were found to have a smooth, apparently featureless surface morphology apart from some randomly dispersed micron size particulates, which we assume to be crystallites that have transported directly from the target following explosive melting of the target surface. The thickness of the deposited P-DLC films was observed to increase with increasing *F*. For example, in the case of films deposited for 20 min at T_{sub} = 298 K, the thickness was found to increase from ~30 nm (for F = 4 J cm^{-2}) to ~50 nm (F = 12 J cm^{-2}).

XPS and LRS have proven to be very useful for characterising the deposited P-DLC films.[11,17] XPS shows peaks attributable to P (2s and 2p), C (1s) and O (1s) (from aerial oxidation). Absolute P : C : O ratios could be determined by comparing the respective peak areas, A_X, weighted by the appropriate atomic sensitivity factors (*i.e.* P : C : O = A_P (2p)/0.39 : A_C/0.25 : A_O/0.66). Such analyses confirm that the stoichiometry of the deposited P-DLC films was sensitive not just to the P : C ratio in the original target, but also to *F* and to T_{sub}. In the case of P-DLC films formed by ablating at F = 12 J cm^{-2} and deposited at T_{sub} = 298 K, for example, the P content of films grown from the 4.1 at.% P in C target was found to be as high as ~8.5 at.%, while those grown by PLA of the 27.9 at.% P in C target contained only ~18 at.% P. Increasing T_{sub} led to a decrease in P content (*e.g.* falling to ~1.5 at.% in the case of films grown at F = 12 J cm^{-2} from the 4.4 at.% P in C target at T_{sub} = 700 K), as did increasing fluence (*e.g.* from 25 to 18 at.% P in the case of films grown from the 27.9 at.% P in C target as *F* was raised from ~4 to ~12 J cm^{-2}).

Such compositional variations, and the observed decline in film thickness as T_{sub} is raised, hint at the complex variety of factors that can, and do, affect the stoichiometry and structure of films grown by PLD methods.[29,30] The target surface in the present experiments is an inhomogeneous mixture of finely divided P and C. Pulsed UV excitation results in local heating in the immediate vicinity of the focal spot on the target surface. The peak temperature, and the duration of the high temperature regime, will depend on *F*. Thus the observed evolution in P : C ratio with *F*, for example, could be rationalised by assuming preferential ablation of the (more volatile) P component at lower target temperatures, and thus lower *F*. In the same vein, the observation that films grown by PLA of dilute P in C targets are enriched in P (relative to the target stoichiometry) could reflect the more rapid, and more localised heating of C-rich targets (graphite having a higher extinction coefficient and melting/boiling temperature than phosphorus), and the consequent higher evaporation rate of 'super-heated' P. Such 'super-heating' would be expected to become less important as the P : C ratio increases, as observed. At high P : C ratio and high *F* the deposited P-DLC films contain a smaller P fraction than the target. The value of *F* will also affect the amount of material removed per shot, and thus the probability of collision induced material processing in the expanding plume of ejected material, the extent of excitation and ionisation of material in the ablation plume, and the mean kinetic energies of the ablated particles – all of which could affect the composition and the microstructure of the deposited film. T_{sub}, of course, cannot affect the ablation event, but it can affect the surface mobility of particles that impact on the substrate, and the relative propensities of their, for example, accommodating, bonding and/or re-bounding back into the gas phase.[29,30] The observed decrease in P : C ratio in P-DLC films grown at higher

T_{sub} may indicate that P atoms are accommodated less efficiently than C during the film growth process.[17]

Fig. 8 presents expanded views of the various P 2p and C 1s XPS peaks measured for P-DLC films deposited at T_{sub} = 298 K (panels (a)–(c) and (d)–(f), respectively). Panel (a) shows the P 2p signal acquired from XPS of a P-DLC film deposited by PLA of a 27.9 at.% P in C target at $F \sim 4$ J cm^{-2}. Two maxima are clearly evident, centred at ~130.7 and ~133.2 eV (indicated by the vertical dashed lines). This splitting, which is considerably larger than the (unresolved) ~1 eV spin–orbit splitting, can be attributed to, respectively, P–P bonding as in red phosphorus[31] and P sites bonded to O[32] (which we presume to be at, or near to, the film surface). No contribution was identified that could be specifically associated with P–C bonding. This accords with the previously noted[17] lack of any resonance specifically attributable to P–C bonding in the laser Raman spectra of these films but does not, in itself, preclude the possibility that a feature attributable to P atoms bonded to C lies within the observed band envelope. Increasing F to ~ 12 J cm^{-2} (panel (b)) leads to a reduction in the absolute signal intensity, and a reduction in the relative size of the signal associated with P–P bonding. This evolution in peak shape is even more evident when using lower P : C ratio targets. Panel (c) shows the P 2p peak measured from a film grown by PLA of the 4.1 at.% P in C target, at $F \sim 12$ J cm^{-2}. The peak at lower energy – attributable to P–P bonding – is now the minor feature. All such observations are consistent with the trends in film P content summarised above: the relative intensity of the measured P–O feature will be particularly sensitive to the near surface P content, and should scale less steeply with P content than the P–P feature.

The right hand panels in Fig. 8 show that the detailed shapes of the corresponding C 1s XPS peaks are also sensitive to the deposition conditions. As previously,[33] we can deconvolute these lineshapes (using Voigt functions) to gain a measure of the ratio of sp^3- to sp^2-bonded carbon in the P-DLC films. We

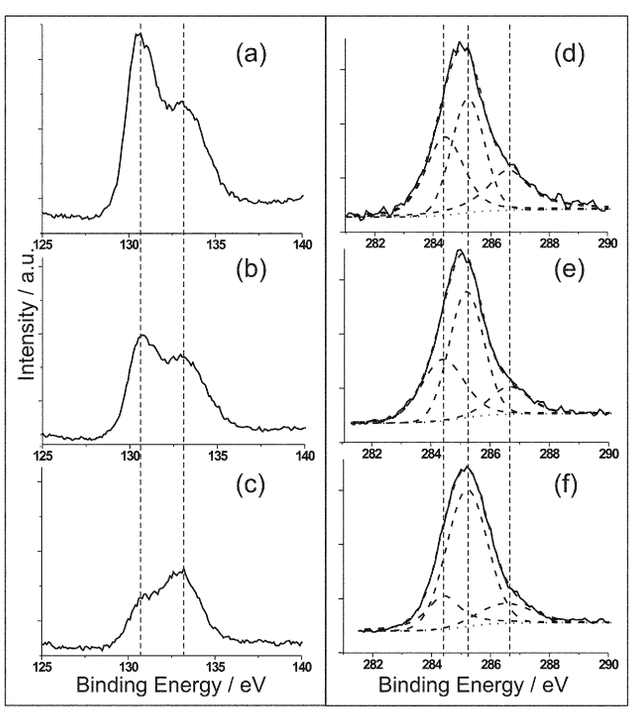

Fig. 8 P 2p and C 1s XPS spectra of P-DLC films deposited at T_{sub} = 298 K following PLA of: 27.9 at.% P in C target at F = 12 J cm^{-2} [(a) and (d)]; 27.9 at.% P in C target (F = 4 J cm^{-2}) [(b) and (e)]; and 4.1 at.% P in C (F = 12 J cm^{-2}) [(c) and (f)]. The two vertical dashed lines on panels (a)–(c) indicate the assumed line centres of the overlapping P–P and P–O peaks, while the vertical lines on spectra (d)–(f) show the assumed C-sp^2, C-sp^3 and C–O band centres. The dashed contributions from C-sp^2 (centred at 284.4 eV), C-sp^3 (285.2 eV) and C–O bonding (~286.5 eV) are indicated by the dashed curves in (d)–(f).

persist with the assumption that these P-DLC films contain little or no P–C bonding, and model the C 1s peak in terms of contributions from C-sp^2 (centred at 284.4 eV), C-sp^3 (285.2 eV) and C–O bonding (~286.5 eV) only. The dashed curves in panels (d)–(f) illustrate such deconvolutions. The results of such deconvolutions are summarised in Fig. 9: the deduced C-sp^3 fraction in the P-DLC films appears to increase gently with F (Fig. 9(a)) – mirroring previously reported behaviour for P-free DLC films,[34] but to decrease with the film P content (Fig. 9(b)).[35] These trends will be considered later, together with our previous observations that the C-sp^3 fraction in such P-DLC films declines with increasing T_{sub}.[11]

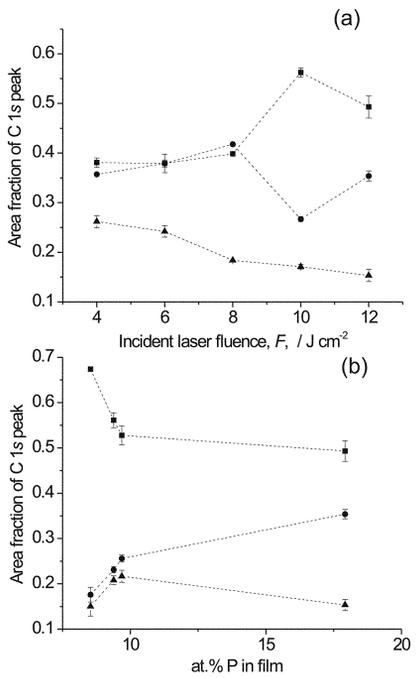

Fig. 9 Plots showing the relative areas of the Voigt functions representing C-sp^2 (●), C-sp^3 (■) and C–O bonding (▲) used to fit the C 1s XPS peak measured for P-DLC films grown at T_{sub} = 298 K as a function of (a) F, from the 27.9 at.% P in C target, and (b) at.% P in the film deposited following PLA at F = 12 J cm^{-2}.

Fig. 10 shows several laser Raman spectra, all recorded at an excitation wavelength of 514.5 nm. Panels (a) and (b) cover the wavenumber range 150–1050 cm^{-1}, while panels (c)–(f) all span the 1000–2000 cm^{-1} region. Panel (a) illustrates the essential similarity between the laser Raman spectrum of a pure red phosphorus sample and that of a thin film of P deposited, by PLD, on an Si substrate, while (b) compares spectra of a Si substrate with and without P-DLC coatings. The two P-DLC films were deposited at T_{sub} = 298 K, using the 27.9 at.% P in C target with different fluences, F = 12 and 4 J cm^{-2}. The broad feature evident in the 320–490 cm^{-1} region is similar to that displayed by the pure phosphorus film and serves to confirm the presence of P in the P-DLC film.[36] More noteworthy, however, is the absence of any obvious feature at ~700 cm^{-1} in the spectrum of the P-DLC film. We have computed calculated vibrational frequencies for a range of organic molecules containing sp^3 and sp^2 carbon, and sp^3 and hypervalent phosphorus atoms in the structural units indicated by the calculations on periodic systems. We have also used DFT and linear response theory to calculate phonon frequencies for pseudo-cubic P_4C_3 at the gamma point. All these calculations[18] indicate P–C stretching frequencies in the range 670–780 cm^{-1}. We have not calculated Raman scattering probabilities, but the lack of any features in this region of the P-DLC film spectrum shown in Fig. 10(b) suggests there is little P–C bonding in the P-DLC films investigated here.

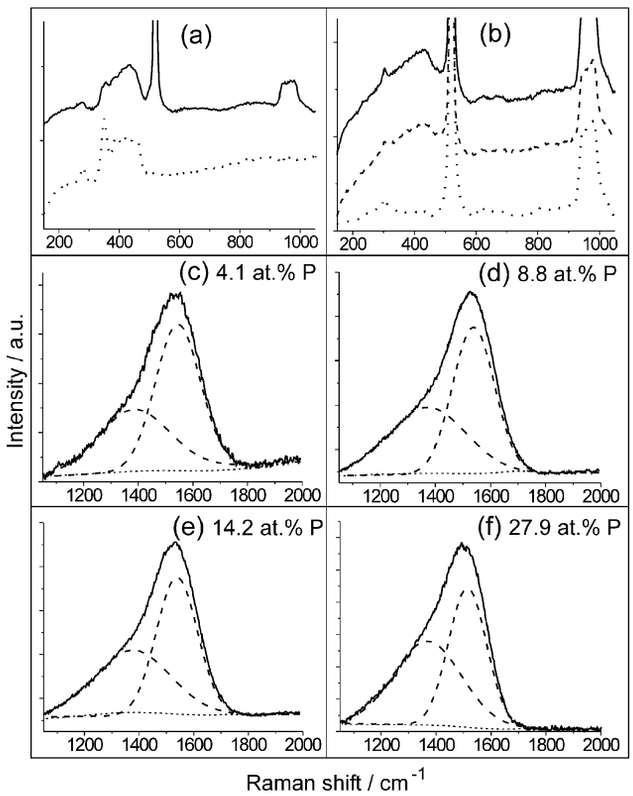

Fig. 10 Laser Raman spectra recorded at an excitation wavelength of 514.5 nm: (a) compares the 150–1050 cm^{-1} regions of spectra of pure red phosphorus (solid line), and (offset vertically for clarity) a film deposited, by PLA of red phosphorus, on Si, at T_{sub} = 298 K (short dashed line); (b) shows spectra of the bare Si substrate (dotted line) and of two P-DLC films deposited on Si, at T_{sub} = 298 K, using the 27.9 at.% P in C target with F = 12 J cm^{-2} (long dashed line) and F = 4 J cm^{-2} (dotted line), (again offset vertically for clarity); (c)–(f) show the 1000–2000 cm^{-1} region of spectra of P-DLC films deposited on Si, in vacuum, using the four different P/C targets as indicated in the figure, F = 12 J cm^{-2} and T_{sub} = 298 K. Each has been fitted using two independent Gaussian functions (long dashed curves) centred at ~1580 and ~1350 cm^{-1}. The short dashed line at $y \sim 0$ in each of panels (c)–(f) shows the residuals of the respective fits.

Panels (c)–(f) in Fig. 10 compare the higher wavenumber region of the laser Raman spectra of P-DLC films, deposited on Si, in vacuum, using the four different P/C targets, an incident fluence, F = 12 J cm^{-2}, and T_{sub} = 298 K. Such peak shapes are characteristic of all graphitic/DLC films, and each has been fitted in terms of two independent Gaussian functions (long dashed curves) centred at ~1580 cm^{-1} (*i.e.* close to the G vibrational mode of graphite, involving an E_{2g} symmetrical bond stretching motion of pairs of sp^2 carbon atoms) and ~1350 cm^{-1} (*i.e.* near the D band associated with the breathing mode of six-membered rings).[37] The short dashed line at $y \sim 0$ in each panel shows the residuals of the respective fits. Quantities of interest include the maxima, G_{max} and D_{max} (in wavenumbers), and the ratio of the relative intensities of the G and D bands, I(G) and I(D). As Fig. 11(a) shows, G_{max} and D_{max} both decline gently with increasing at.% P in the deposited film and, for any given at.% P, increase with F. The I(D)/I(G) ratios determined for all P-DLC films grown by PLA of C/P containing targets are significantly greater than those for undoped DLC films grown under otherwise equivalent conditions (and analysed at the same Raman excitation wavelength) – for which (I(D)/I(G) is typically ~0.2,[33] but still much lower than the ratios measured for DLC and doped DLC films grown at high T_{sub} – which can be >1.5.[11,33,37] Fig. 11(b) illustrates the deduced increase in the I(D)/I(G) ratio with at.% P content in the film. These latter observations mimic trends noted previously in the case of N-doped DLC films[33,38–41] and are generally taken as indications of an increased

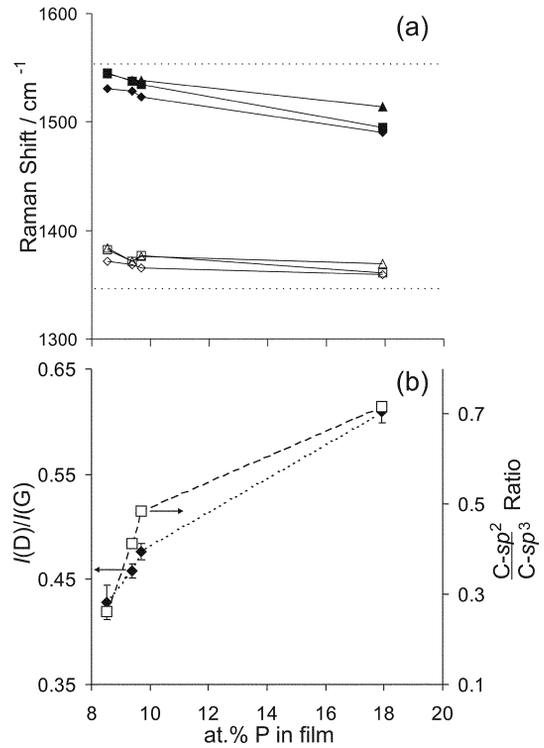

Fig. 11 Deduced variation with at.% P in P-DLC films deposited on Si, in vacuum, at T_{sub} = 298 K, of: (a) G_{max} (closed symbols) and D_{max} (open symbols), for a range of F (F = 4 J cm^{-2} (◆), 8 J cm^{-2} (■) and 12 J cm^{-2} (▲)). For reference, the horizontal dashed lines indicate the G_{max} and D_{max} band centres for crystalline graphite. (b) I(D)/I(G) ratio (◆, left hand scale) and C-sp^2/C-sp^3 ratio (□, right hand scale) at F = 12 J cm^{-2}.

propensity for forming islands of nanocrystalline graphite and, possibly, fullerene-like structures within an (in this case, phosphorus containing) amorphous carbon matrix. Further support for such a view is provided by the deconvolutions of the C 1s XPS peaks summarised in Fig. 8(d)–(f) which, as Fig. 11(b) shows, reveal a systematic increase in C-sp^2/C-sp^3 ratio with increasing at.% P in the deposited film (at least for ≤18 at.% P).

Conclusions

This paper presents computational results relating to crystalline phosphorus carbide bulk phases and experimental studies of amorphous C/P containing thin films, with a maximum P content of 27.9 at.%. The *ab initio* DFT studies of PC_3 suggest that, as for PC, but unlike P_4C_3, there exists a set of possible structures all of which lie close in energy. Such a finding may offer some rationale for our failure to discern any evidence for crystalline carbon phosphide or, indeed, even any unequivocal evidence for P–C bonding in films grown on Si substrates following PLA of several different C/P containing targets.

Much remains to be done. One key goal is to establish, unambiguously, the presence of P–C bonding in such deposits, and then to try and enhance the crystallinity of the material. Possible strategies include impacting high energy C atoms (such as are produced in PLA of graphite in vacuum) into a phosphorus substrate, ablation of P targets under a carbon containing liquid (inspired by reports of pulsed laser induced formation of nanodiamond at an acetone/graphite interface[42]) and/or more traditional high temperature, high pressure (HPHT) synthetic routes. Such experimental progress, in turn, would enable much closer contact between theory and experiment. We anticipate that the exploratory work presented here will encourage further wide ranging experimental and theoretical investigations of binary phosphorus–carbon compounds.

Acknowledgements

The authors are all pleased to acknowledge the financial support for this work provided by EPSRC. We are also very grateful to Dr M. Chhowalla (Cambridge University) for help with C/P target preparation, and to K. N. Rosser, J. Filik, Dr S. R. J. Pearce and staff of the mechanical and electronics workshops in the School of Chemistry and of the Interface Analysis Centre at the University of Bristol for their many and varied contributions to the work described herein.

References

1 D. M. Teter and R. J. Hemley, *Science*, 1996, **271**, 53, and references therein.
2 C. M. Niu, Y. Z. Lu and C. M. Lieber, *Science*, 1993, **261**, 334.
3 A. A. Voevodin, J. G. Jones, J. S. Zabinski, Z. Czigany and L. Hultman, *J. Appl. Phys.*, 2002, **92**, 4980.
4 Z. M. Zhou and L. F. Xia, *J. Phys. D: Appl. Phys.*, 2002, **35**, 1991.
5 C. Popov, M. F. Plass, R. Kassing and W. Kulisch, *Thin Solid Films*, 1999, **356**, 406.
6 T. Komatsu, *J. Mater. Chem.*, 2001, **11**, 799.
7 Q. Guo, Y. Xie, X. Wang, S. Zhang, T. Hou and S. Lv, *Chem. Commun.*, 2004, 26.
8 S. R. J. Pearce, P. W. May, R. K. Wild, K. R. Hallam and P. J. Heard, *Diamond Rel. Mater.*, 2002, **11**, 1041.
9 F. Claeyssens, N. L. Allan, P. W. May, P. Ordejón and J. M. Oliva, *Chem. Commun.*, 2002, 2494.
10 F. Claeyssens, J. M. Oliva, P. W. May and N. L. Allan, *Int. J. Quantum Chem.*, 2003, **95**, 546.
11 G. M. Fuge, P. W. May, K. N. Rosser, S. R. J. Pearce and M. N. R. Ashfold, *Diamond Rel. Mater.*, 2004, **13**, 1442.
12 J. P. Perdew and Y. Wang, *Phys. Rev. B*, 1992, **45**, 13244.
13 CASTEP 4.2 academic version, licensed under the UKCP-MSI agreement, 1999, *Rev. Mod. Phys.*, 1992, **64**, 1045.
14 D. Vanderbilt, *Phys. Rev. B*, 1990, **41**, 7892.
15 J. M. Soler, E. Artacho, J. D. Gale, A. García, J. Junquera, P. Ordejón and D. Sánchez-Portal, *J. Phys: Condens. Matter*, 2002, **14**, 2745.
16 J. P. Perdew, K. Burke and M. Ernzerhof, *Phys. Rev. Lett.*, 1996, **77**, 3865.
17 F. Claeyssens, G. M. Fuge, N. L. Allan, P. W. May, S. R. J. Pearce and M. N. R. Ashfold, *Appl. Phys. A*, in press.
18 F. Claeyssens, N. L. Allan, J. M. Oliva and P. W. May, manuscript in preparation.
19 M. Mattesini and S. F. Matar, *Phys. Rev. B*, 2002, **65**, 75110.
20 M. Côté and M. L. Cohen, *Phys. Rev. B*, 1997, **55**, 5684.
21 É. Sandré, C. J. Pickard and C. Colliex, *Chem. Phys. Lett.*, 2000, **325**, 53.
22 N. N. Greenwood and A. Earnshaw, *Chemistry of the Elements*, Butterworth-Heinemann, Oxford, 1997.
23 J. C. Zheng, M. C. Payne, Y. P. Feng and A. T. L. Lim, *Phys. Rev. B*, 2003, **67**, 153105.
24 *E.g.*, H. H. Karsch and E. Witt, *J. Organomet. Chem.*, 1997, **529**, 151.
25 I. N. Remediakis and E. Kaxiras, *Phys. Rev. B*, 1999, **59**, 5536.
26 M.-T. Kuo, P. W. May, A. Gunn, M. N. R. Ashfold and R. K. Wild, *Diamond Rel. Mater.*, 2000, **9**, 1222.
27 S. R. J. Pearce, J. Filik, P. W. May, R. K. Wild, K. R. Hallam and P. J. Heard, *Diamond Rel. Mater.*, 2003, **12**, 979.
28 G. Fasol, M. Cardona, W. Hönle and H. G. von Schnering, *Solid State Commun.*, 1984, **52**, 307.
29 *Pulsed Laser Deposition of Thin Films*, ed. D. B. Chrisey and G. K. Hubler, John Wiley and Sons, New York, 1994.
30 M. N. R. Ashfold, F. Claeyssens, G. M. Fuge and S. J. Henley, *Chem. Soc. Rev.*, 2004, **33**, 23, and references therein.
31 *Handbook of X-ray Photoelectron Spectroscopy*, Physical Electronics Division, Perkin Elmer Corp., Eden Prairie, MN, 1992.
32 R. Imamura, K. Matsui, S. Takeda, J. Ozaki and A. Oya, *Carbon.*, 1999, **37**, 261.
33 G. M. Fuge, C. J. Rennick, S. R. J. Pearce, P. W. May and M. N. R. Ashfold, *Diamond Rel. Mater.*, 2003, **12**, 1049.
34 P. Mérel, M. Tabbal, M. Chaker, S. Moisa and J. Margot, *Appl. Surf. Sci.*, 1998, **136**, 105.
35 B. Kleinsorge, A. C. Ferrari, J. Robertson, W. I. Milne, S. Waidmann and S. Hearne, *Diamond Rel. Mater.*, 2000, **9**, 643.
36 D. J. Olego, J. A. Baumann, M. A. Kuck, R. Schachter and C. G. Michel, *Solid State Commun.*, 1984, **52**, 311.
37 A. C. Ferrari and J. Robertson, *Phys. Rev. B*, 2000, **61**, 14095, and references therein.
38 Y. H. Cheng, X. L. Qiao, J. G. Chen, Y. P. Wu, C. S. Xie, Y. Q. Wang, D. S. Xu, S. B. Mo and Y. B. Sun, *Diamond Rel. Mater.*, 2002, **11**, 1511.
39 C. W. Ong, X.-A. Zhao, Y. C. Tsang, C. L. Choy and P. W. Chan, *Thin Solid Films*, 1996, **280**, 1.
40 X.-A. Zhao, C. W. Ong, Y. C. Tsang, K. F. Chan, C. L. Choy, P. W. Chan and R. W. M. Kwok, *Thin Solid Films*, 1998, **333**, 245.
41 M. E. Ramsey, E. Poindexter, J. S. Pelt, J. Marin and S. M. Durbin, *Thin Solid Films*, 2000, **360**, 82.
42 J. B. Wang, C. Y. Zhang, X. L. Zhong and G. W. Yang, *Chem. Phys. Lett.*, 2002, **361**, 86.